NDT&E International 44 (2011) 247–253

Contents lists available at ScienceDirect

NDT&E International

journal homepage: www.elsevier.com/locate/ndteint

Measurement of the Rayleigh wave polarization using 1D Laser vibrometry

N. Apetre [a,*], M. Ruzzene [a], L.J. Jacobs [b], J. Qu [c]

[a] School of Aerospace Engineering, Georgia Institute of Technology, Atlanta, GA, United States
[b] School of Mechanical Engineering, Georgia Institute of Technology, Atlanta, GA, United States
[c] Department of Civil and Environmental Engineering, Northwestern University, Evanston, IL, United States

ARTICLE INFO

Article history:
Received 7 January 2010
Received in revised form
26 July 2010
Accepted 30 July 2010
Available online 20 August 2010

Keywords:
Rayleigh wave
Wave polarization
Residual stresses
Scanning Laser Doppler Vibrometer
Ultrasonics

ABSTRACT

The paper presents measurement procedures for the evaluation of velocity/displacement components of surface elastic waves through a single beam Laser Vibrometer. The developed technique is applied for the estimation of Rayleigh wave polarization in aluminum specimens. The estimated polarization orbits are compared with the analytical ones to demonstrate the effectiveness of the measurement technique. The estimations rely on the preliminary analysis of the recorded signals in the frequency/wavenumber domain, as enabled by the fine spatial resolution provided by a scanning Laser vibrometer, which allows identification and separation of Rayleigh waves from the recorded wavefield. In addition, comparison of polarization measurements performed on untreated and shot-peened samples suggests the measurement technique as a tool for the estimation of the effect of residual stresses on the polarization properties of surface waves.

Published by Elsevier Ltd.

1. Introduction

Polarization defines the phase and amplitude relationships between the various components of wave motion, and is significant in all technological applications based on wave propagation, such as optics, seismology, telecommunications and radar science. As opposed to other fields, wave polarization in mechanics has received relatively little attention, due to the general difficulty in evaluating it experimentally. It is, however, a well-recognized fact that the ability to measure and characterize the polarization of ultrasonic waves could lead to the development of novel diagnostic tools, which could rely on the sensitivity of polarization to surface roughness, cracks, temperature or residual stresses, among others. For example, the acousto-elastic effect, which describes the dependency of ultrasonic wave speed and polarization on state of stress, is a well-known phenomenon that has been extensively reported in the literature [1,2]. The use of the acousto-elastic effect for the estimation of residual stresses through wave speed measurement is an attractive technique which, however, requires exact knowledge of the distance between transducer and receiver [3], and which provides a relative measurement as opposed to an absolute one [4]. Lack of sensitivity of wave velocity measurements has also been reported as a potential issue. The theoretical study of the polarization of Rayleigh surface waves presented in [5], suggests an alternative method for surface stress estimation. A "polarization parameter" defined as the ratio between the maximum in-plane and out-of-plane displacement components is directly related to the state of stress, and could therefore be used as an absolute measurement of residual stresses. Studies on the acousto-elastic effect on Rayleigh waves in a homogeneous material include the work of Hirao et al. [6], while Duquennoy et al. [7,8] also investigated the influence of residual stresses on Rayleigh waves propagation.

Recently, Scanning Laser Doppler Vibrometers (SLDV) have found broad application for the detailed measurement and characterization of ultrasonic wavefields [9,10]. The limitation of 1D-SLDVs to measure a single displacement component parallel to the incident Laser beam can be overcome by the use of three-dimensional SLDVs (3D-SLDV), which provide the ability to resolve the three components of the wavefield. As an alternative, the resolution of the displacement components can also be achieved through 1D-SLDVs by repeating the experiments at various angles of incidence, provided knowledge of such angles and of the location of the specimen with respect to the Laser head. This approach, which has been demonstrated and presented in [11,12], is very attractive since it avoids the large equipment costs associated with 3D-SLDVs and their hardware. Specifically in [12], the three velocity components of Lamb and Shear Horizontal waves are evaluated through three 1D-SLDV measurements, and subsequently post-processed to investigate the interaction of Lamb waves with damage in composite plates.

The current paper applies a similar approach as in [12] to demonstrate the feasibility of 1D-SLDV for wave polarization measurements. The study focuses on the Rayleigh wave, for which

* Corresponding author.
E-mail address: nicole.apetre@gatech.edu (N. Apetre).

0963-8695/$ - see front matter Published by Elsevier Ltd.
doi:10.1016/j.ndteint.2010.07.007

measured polarizations are compared with analytical ones as presented in classical reference books [5]. The polarization estimations rely on the preliminary identification and separation of the various wave modes, which is achieved through filtering in the wavenumber domain, which is enabled by the spatial resolution provided by the SLDV. The results presented in terms of elliptical orbits show excellent correlation with the analytical predictions, and suggest the application of the developed measurement technique both for wavefield characterization, and for the detection of changes in the polarization properties of the media resulting from a state of prestress and/or damage. To this end, preliminary results are here presented to compare the measured polarization in specimens treated with different shot-peening intensities. The obtained polarization orbits appear to be strongly affected by the surface state of pre-stress, which suggests the possibility of using polarization as a way to characterize the state of surface stress as suggested in [4].

The paper is structured as follows. First, a discussion of the theoretical background which forms the basis of these techniques is presented in Section 2. The application to Rayleigh wave experimental data is then illustrated in Section 3 whereas, Section 4 summarizes the main results of the work and recommends areas of future investigations.

2. Experimental approach for the measurement of wave polarization

This section presents the methodology used to determine in-plane and out-of-plane components of the experimental data. A short introduction on the experimental set-up is presented, followed by an analytical description of the method.

2.1. Laser vibrometry for wavefield detection

A schematic of the considered experimental set-up is shown in Fig. 1. The experimental data are obtained using piezoceramic discs as actuators, and a Scanning Laser Doppler Vibrometer (SLDV) as a sensor. The SLDV (Polytec PI, Model PSV400M2) allows frequency sampling up to 1 MHz, which enables ultrasonic waves detection and visualization. In the wave propagation tests, the piezo discs are driven by a sinusoidal burst generated by a signal generator. The resulting elastic waves are recorded at the measurement grid points defined on the scanning system. The operation of the SLDV requires the generation of a pulse at each grid point in order to record the corresponding response. Phase information is retained by triggering the excitation signal through a low frequency signal (10 Hz), which also defines the scanning rate. Upon completion of measurements at all grid points, the recorded responses are post-processed to obtain full images of the propagating wavefield within the region of inspection.

2.2. Estimation of in-plane and out-of-plane components

The 1D-SLDV measures velocity and displacements of the surface under consideration in the direction aligned with the Laser beam. Consider the configuration shown in Fig. 2, which presents a schematic of the experimental set-up used for this study. Let the orientation of the specimen with respect to the Laser beam be described by the angle θ, which is formed between the unit vector $\boldsymbol{i}_1$ along the surface of the specimen, and the unit vector $\boldsymbol{i}_L$ aligned with the Laser beam. The response of the specimen to an excitation provided by the source S is measured at a number of points located along the scan line, which is defined by an initial point I and a final point F. For simplicity, we assume that the origin of the axis x_1 is located at point O which corresponds to the point illuminated by a Laser beam parallel to the X axis fixed to the Laser head. In Fig. 2, d defines the distance between the Laser head and the specimen measured along the X axis. Knowledge of such distance is needed for the estimation procedure described in what follows.

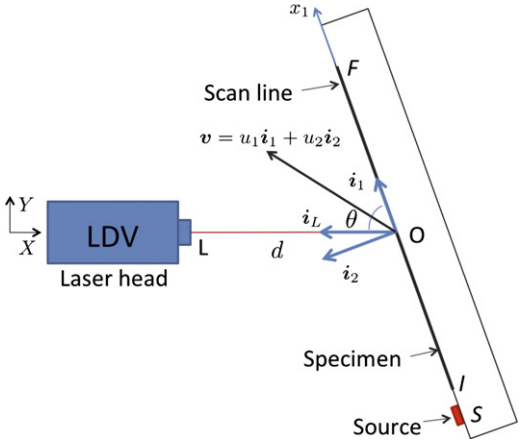

Fig. 2. Experimental set-up and main geometrical variables.

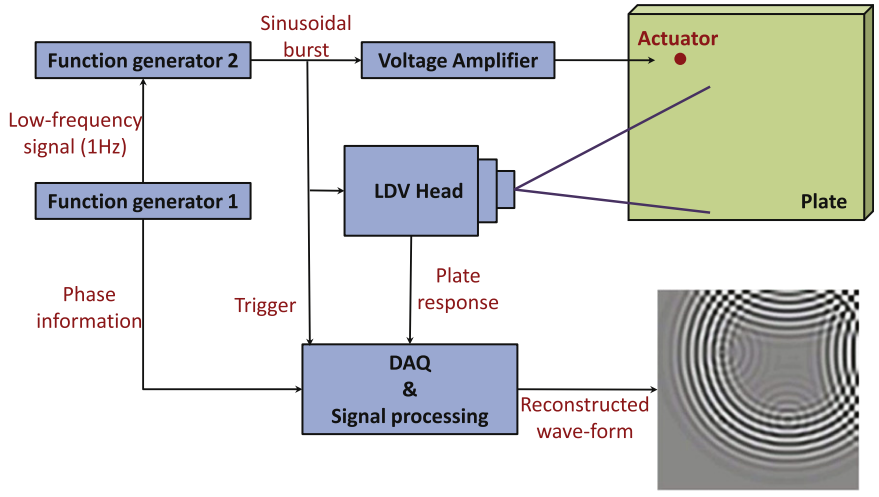

Fig. 1. Schematic of experimental set-up for wavefield measurement.

First, the estimation of in-plane and out-of-plane components is illustrated for point O and it is then extended for a generic point K located at $x_{1_k} \in [x_{1_I}, x_{1_F}]$. The description is here based on velocity components, with the understanding that a similar procedure generates the displacement components should displacement data be provided as a result of the experiments. Let the velocity of point O be expressed as

$$\boldsymbol{v}(x_{1_o}) = u_1(x_{1_o})\boldsymbol{i}_1 + u_2(x_{1_o})\boldsymbol{i}_2 \tag{1}$$

where u_1, u_2 denote the in-plane and out-of-plane components of the velocity at the point O. The LDV measures the component of the velocity parallel to the beam, which is denoted as u_L, and which can be expressed in terms of u_1, u_2 by

$$u_L(x_{1_o}) = \boldsymbol{v}(x_{1_o}) \cdot \boldsymbol{i}_L \tag{2}$$

which, given that $\boldsymbol{i}_L = \cos\theta \boldsymbol{i}_1 + \sin\theta \boldsymbol{i}_2$, yields

$$u_L(x_{1_o}) = u_1(x_{1_o})\cos\theta + u_2(x_{1_o})\sin\theta \tag{3}$$

Given that u_L is known as provided by the LDV, while u_1, u_2 need to be determined, two measurements at two orientation angles θ_a, θ_b need to be performed in order to obtain two equations of the kind of Eq. (3). This leads to the following system:

$$\begin{Bmatrix} u_L^{(a)}(x_{1_o}) \\ u_L^{(b)}(x_{1_o}) \end{Bmatrix} = \begin{bmatrix} \cos\theta_a & \sin\theta_a \\ \cos\theta_b & \sin\theta_b \end{bmatrix} \begin{Bmatrix} u_1(x_{1_o}) \\ u_2(x_{1_o}) \end{Bmatrix} \tag{4}$$

and

$$\begin{Bmatrix} u_{1_o} \\ u_{2_o} \end{Bmatrix} = \frac{1}{\sin(\theta_a - \theta_b)} \begin{bmatrix} -\sin\theta_b & \sin\theta_a \\ \cos\theta_b & -\cos\theta_a \end{bmatrix} \begin{Bmatrix} u_{L_o}^{(a)} \\ u_{L_o}^{(b)} \end{Bmatrix} \tag{5}$$

Eq. (5) shows the importance of the proper selection of the orientation angles θ_a, θ_b, that need to differ substantially to avoid indeterminacy of the two velocity components. Their value must also consider the limited sensitivity of the LDV which is optimal at normal angular incidence ($\theta = 90^\circ$).

The value of the angles to be used in Eq. (5) needs to be corrected when the velocity components are evaluated at locations other than O (Fig. 3). The measured velocity at point K is given by

$$u_L(x_{1_K}) = \boldsymbol{v}(x_{1_K}) \cdot \boldsymbol{i}_{L_K} \tag{6}$$

which is expressed in terms of the corresponding in-plane and out-of-plane components through the following relation:

$$u_{L_K} = u_1(x_{1_K})\cos\theta_k + u_2(x_{1_K})\sin\theta_k \tag{7}$$

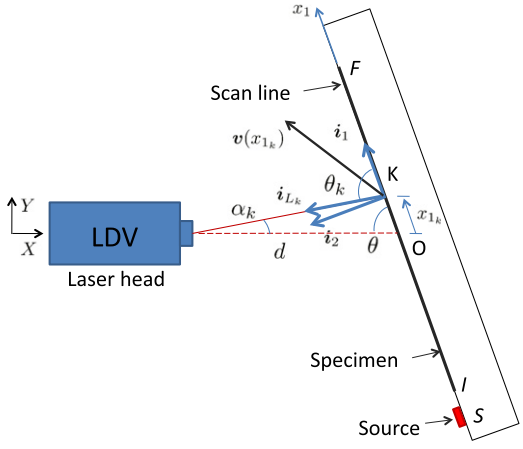

Fig. 3. Experimental set-up and main geometrical variables.

The angle θ_k depends on the location of point K with respect to point O, the distance between the Laser head and the specimen, and the orientation angle θ as defined by the following expression:

$$\theta_k = \begin{cases} \theta + \tan^{-1}\left[\dfrac{x_{1_k}\sin\theta}{d - x_{1_k}\cos\theta}\right] & \text{if K is above O} \\ \tan^{-1}\left[\dfrac{d\sin\theta}{x_{1_k} + d\cos\theta}\right] & \text{if K is below O} \end{cases} \tag{8}$$

3. Rayleigh wave experiments

This section presents the computation of Rayleigh wave polarization in aluminum specimens. A short introduction on the experimental set-up is followed by the application of the method to experimental data.

3.1. Experimental set-up

Experiments are performed on thick aluminum blocks, where elastic waves are generated through a surface mounted piezo-electric disc. The discs are excited by a narrowband pulse in the frequency range 10–500 kHz using a pulser-receiver (Olympus Model 5058 PR). Fig. 4 shows the specimen with the surface mounted piezo used for its excitation. The surface response of the specimen is recorded along a straight line originating from the source. Measurements are repeated at different angles so that in-plane and out-of-plane displacement components can be estimated. This is achieved by mounting the aluminum block on an optical table, which allows orienting it at specified angles with respect to the Laser beam. The configuration considers the Laser head in a fixed position, while the specimen is rotated with respect to it at desired angles. The selected orientations are based on the need to maximize angular differences between two sets of measurements to avoid ill-conditioning of the matrices used for the estimation of the in-plane and out-of-plane displacement wavefield components (5). In the experiments, angles of 52.5°, 127.5°, and 90° are chosen, the latter being used as a baseline to verify that the out-plane components estimated through the procedure described in Section 2 match with those measured directly at a normal angle ($\theta = 90^\circ$ in Fig. 2). A strip of reflective

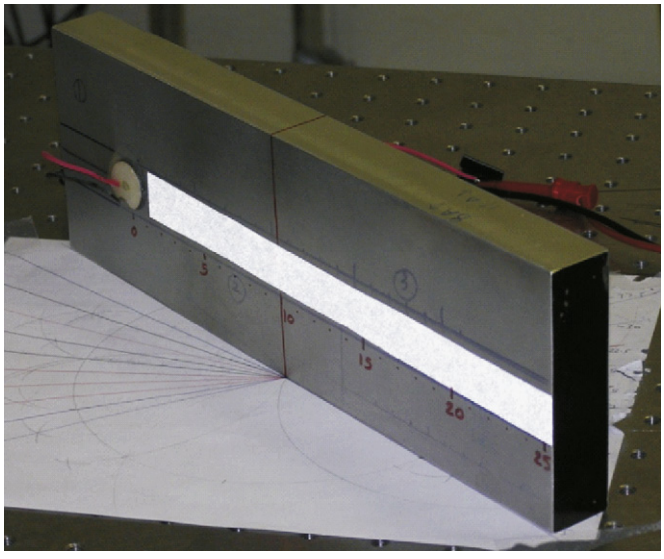

Fig. 4. Specimen for Rayleigh wave polarization measurements.

tape (visible in Fig. 4) is added on the specimen along the scan line in order to achieve good measurement sensitivity for the Laser.

3.2. Wavefield analysis and Rayleigh wave identification

Examples of recorded signals are shown in Fig. 5 in the form of a waterfall plot, which shows the response time histories at 13 evenly spaced locations along the scan line. The displayed responses, recorded directly from the Laser acquisition system, show the complexity of the wavefield, which features one clear direct arrival followed by multiple reflections. Such complexity requires that several signal processing steps are carried out in order to identify and extract the Rayleigh waves from the recorded signals. The fine spatial resolution provided by the Laser Vibrometer allows the application of the 2D Fourier Transform (2D-FT) for the visualization of the line-scan response in the frequency/wavenumber (ω–k) domain. Fig. 6 shows the amplitude of the 2D-FT corresponding to the time traces in Fig. 5 which is an effective way to visualize their modal content. Contour plots of the kind of Fig. 6 can be used to visualize the dispersion relations of the considered medium by following the ridges of the amplitude maxima. In this case, the dashed line of Fig. 6 intercepts a number of peaks in the ω–k diagram and identifies a non-dispersive mode. This mode's phase velocity, estimated as the slope of the dashed line, is $c_{ph}=2957$ m/s. This value is very close to the theoretical one for the Rayleigh waves in aluminum ($E=71$ GPa, $\rho=2700$ kg/m^3, $\nu=0.3$), which is $c_{ph}\approx 2950$ m/s [13]. The non-dispersive nature of this mode and the associated phase velocity strongly suggest that the dashed line identifies the amplitude peaks corresponding to Rayleigh wave propagation. Based on these observations, the Rayleigh wave components can be isolated from the entire wavefield through simple windowing operations in the ω–k domain as described in the following section.

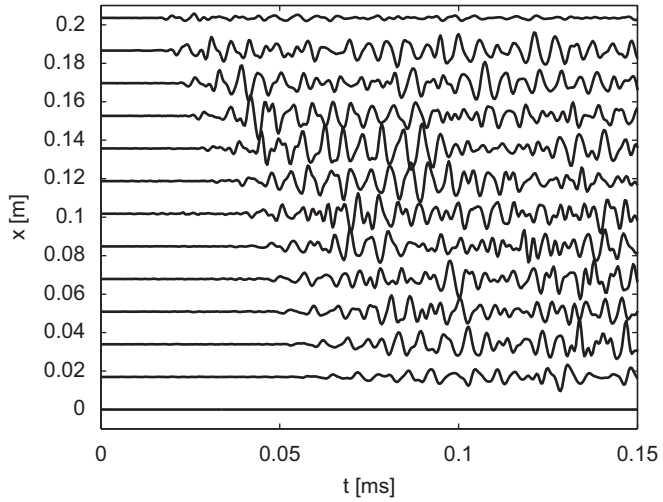

Fig. 5. Specimen response recorded at selected locations along the scan line.

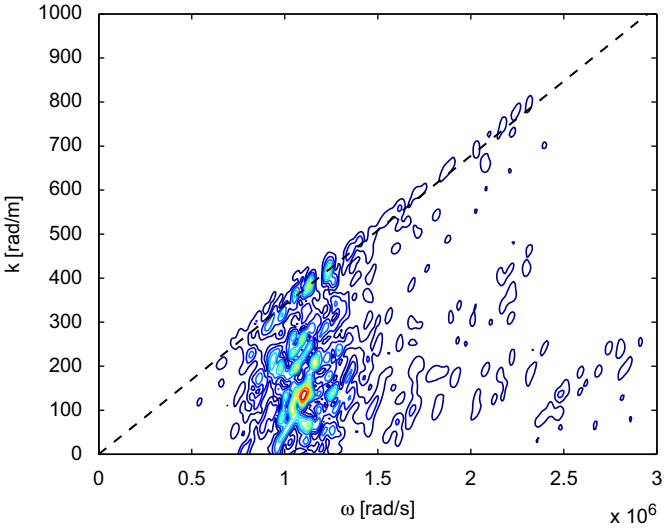

Fig. 6. 2D FT of line-scan response.

3.3. Frequency/wavenumber filtering for separation of the Rayleigh wave mode

The procedure followed for the separation of the Rayleigh wave mode is applied to the data directly recorded from the Laser system, prior to estimating its in-plane and out-of-plane components. Let us denote the recorded line-scan data as $u_L(x_j,t)$, while u_1,u_2 indicate the corresponding in-plane and out-of-plane components, according to the notation introduced in Section 2.2. The time domain waveform data $u_L(x_j,t)$ are first transformed in the ω–k domain by

$$U_L(k,\omega)=\mathcal{F}_{2D}[u_L(x_j,t)] \tag{9}$$

where $\mathcal{F}_{2D}$ is the 2D-FT. The frequency–wavenumber domain data $U_L(k,\omega)$ are then filtered through a window function $\mathcal{W}(k,\omega)$ to give

$$U_{L_{\mathcal{W}}}(k,\omega)=U_L(k,\omega)\mathcal{W}(k,\omega) \tag{10}$$

where $U_{L_{\mathcal{W}}}$ denotes the filtered response. The considered window is given by the product $\mathcal{W}(k,\omega)=\mathcal{W}_1(k,\omega)\mathcal{W}_2(k,\omega)$, to express the concept that a two-step filtering process is performed. The first window $\mathcal{W}_1$ is defined as follows:

$$\mathcal{W}_1(k,\omega)=\begin{cases}0 & |k(\omega)-\omega/c_{ph}|<2w(\omega)\\ 0.5+0.5\cos\left[\dfrac{\pi(k(\omega)-\omega/c_{ph})}{w(\omega)}\right] & |k(\omega)-\omega/c_{ph}|>2w(\omega)\end{cases} \tag{11}$$

Eq. (11) defines a Hann window of width 2w, centered at the wavenumber $k_0=\omega/c_{ph}$, where c_{ph} is the slope of the dashed line corresponding to the Rayleigh wave component in Fig. 6. The width of the window can generally vary as a function of frequency, or, as in this case, can be a constant value. The width w=75 rad/m is selected to perform a narrow filtering process around the dispersion branch of interest. Fig. 7(a) shows the bounds of the window centered on the Rayleigh line. Finally, band-pass filtering limits the analysis to the frequency range where most of the energy of the response is localized. The second Hann window $\mathcal{W}_2$ operates solely in the frequency domain and it is defined as

$$\mathcal{W}_2(k,\omega)=\begin{cases}0 & |\omega-\omega_0|<2\mathrm{w}\\ 0.5+0.5\cos\left[\dfrac{\pi(\omega-\omega_0)}{\mathrm{w}}\right] & |\omega-\omega_0|>2\mathrm{w}\end{cases} \tag{12}$$

where $2\mathrm{w}=0.7\times10^6$ rad/s, and $\omega_0=1.15\times10^6$. The final result of the filtering process is displayed in Fig. 7b.

3.4. Polarization plots

The filtered data are transformed back into the temporal/spatial domain through an inverse 2D FT:

$$u_{L_{\mathcal{W}}}(x_j,t)=\mathcal{F}_{2D}^{-1}[U_{L_{\mathcal{W}}}(k,\omega)] \tag{13}$$

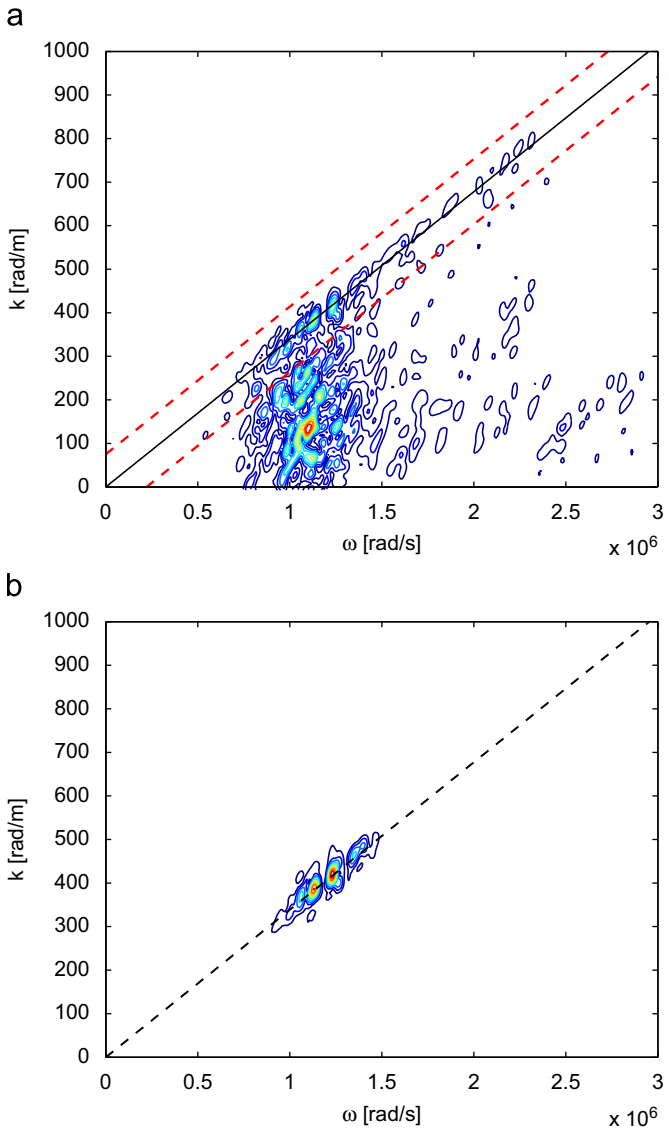

Fig. 7. 2D FT of line-scan response with limits of the frequency/wavenumber filtering window (red dashed lines) (a), and 2D FT of line-scan response upon filtering. (For interpretation of the references to colour in this figure legend, the reader is referred to the web version of this article.)

A rectangular temporal window is finally applied to extract the first arrival and to eliminate subsequent reflections. The result of this operation is displayed in Fig. 8, which clearly shows how the response is considerably cleaner and therefore simple to analyze for the extraction of the in-plane and out-of-plane components.

The procedure presented in Section 2.2 is applied by selecting signals recorded at two different angles. In order to evaluate the effectiveness of the estimation procedure as well as the quality of the experimental set-up, the process first considers angles $\theta_a = 90^\circ$, $\theta_b = 127.5^\circ$, and then $\theta_a = 52.5^\circ$, $\theta_b = 127.5^\circ$. Estimated in-plane and out-of-plane components, denoted, respectively, as u_1 and u_2, are compared in Fig. 9, where the solid line corresponds to the results obtained with the first pair of angles, while the circles are related to the second pair. The comparison, which is performed at a point located approximately at 5 cm from the source, shows an excellent agreement between the two estimations and provides confirmation of the validity of the approach. Similar levels of agreement can be found at other locations, and related plots are omitted for the sake of brevity.

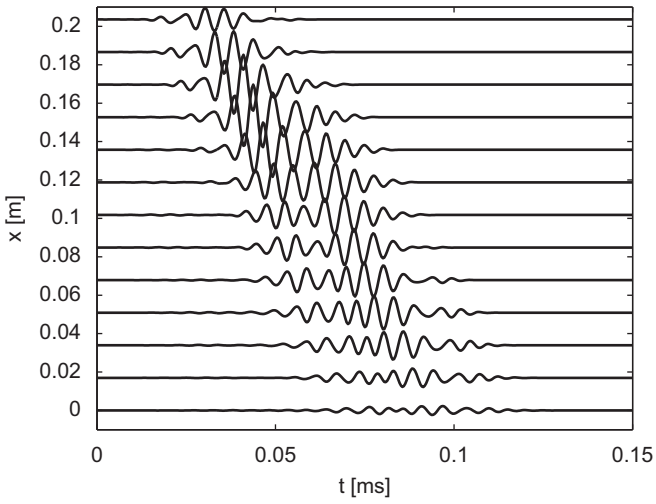

Fig. 8. Specimen response recorded at selected locations along the scan line.

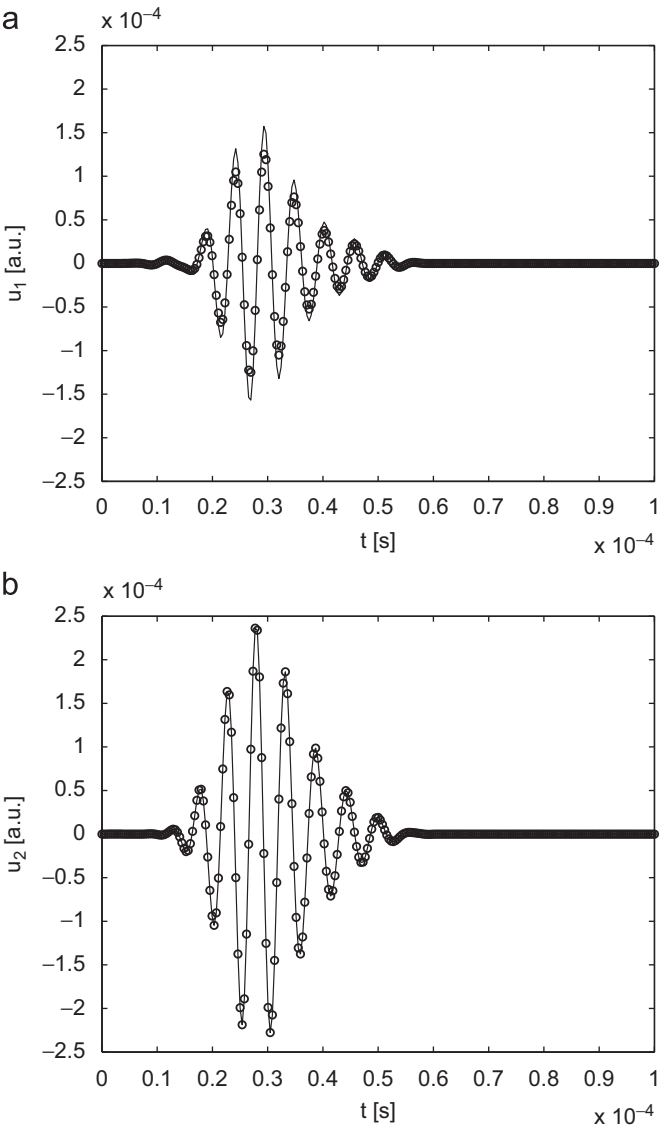

Fig. 9. In-plane ($u_1(t)$) (a) and out-of-plane ($u_2(t)$) (b) components estimated using two pairs of measurement angles ($\theta_a = 90^\circ$, $\theta_b = 127.5^\circ$ solid line, and $\theta_a = 37.5^\circ$, $\theta_b = 127.5^\circ$ dotted line).

Wave polarization is evaluated by tracing particle trajectories through plots of the evolutions of the in-plane versus the out-of-plane components. The plots are generated for curves of the kind shown in Fig. 9, upon proper normalization. The experimental trajectories are compared with those predicted analytically from the theory presented in [5]. Specifically, the analytical estimations are based on the surface displacement components given by

$$u_1(x_1,x_2=0,t)=A[k^2+s^2\beta^2]^{1/2}\sin[k(c_Rt-x_1)]$$

$$u_2(x_1,x_2=0,t)=A[r^2+k^2\beta^2]^{1/2}\cos[k(c_Rt-x_1)] \quad (14)$$

where A and B are constants, $\beta=B/A$, c_R is the speed of Rayleigh waves, k is the corresponding wavenumber, $r=k[1-(c_R/c_d)^2]^{1/2}$, $s=k[1-(c_R/c_s)^2]^{1/2}$, c_d and c_s, respectively, denote the speeds of dilatational and shear waves in the medium.

Eq. (14) can be used to define the polarization trajectories, which can be traced by plotting one component versus the other at a given location x_1, and for increasing time. For comparison with the experimental results, both components are normalized with respect to the amplitude of the out-of-plane displacement, so that the following parametric expressions for the trajectory are considered:

$$\hat{u}_1(x_1,x_2=0,t)=\frac{[k^2+s^2\beta^2]^{1/2}}{[r^2+k^2\beta^2]^{1/2}}\sin\gamma$$

$$\hat{u}_2(x_1,x_2=0,t)=\cos\gamma \quad (15)$$

where γ is a phase angle increasing with time at the considered location, which is varied in the $[0,2\pi]$ interval for plotting purposes.

Experimentally, the particle trajectory at a given location x_k are estimated by considering the two components, normalized with respect to the amplitude of one of the them evaluated at each instant of time. Specifically, the trajectory is estimated by plotting the normalized out-of-plane component $\hat{u}_2(x_{i_k},t)$ versus the normalized in-plane component $\hat{u}_1(x_k,t)$, which are respectively defined as

$$\hat{u}_1(x_k,t)=\frac{u_1(x_k,t)}{\|\tilde{u}_2(x_k,t)\|}$$

$$\hat{u}_2(x_k,t)=\frac{u_2(x_k,t)}{\|\tilde{u}_2(x_k,t)\|} \quad (16)$$

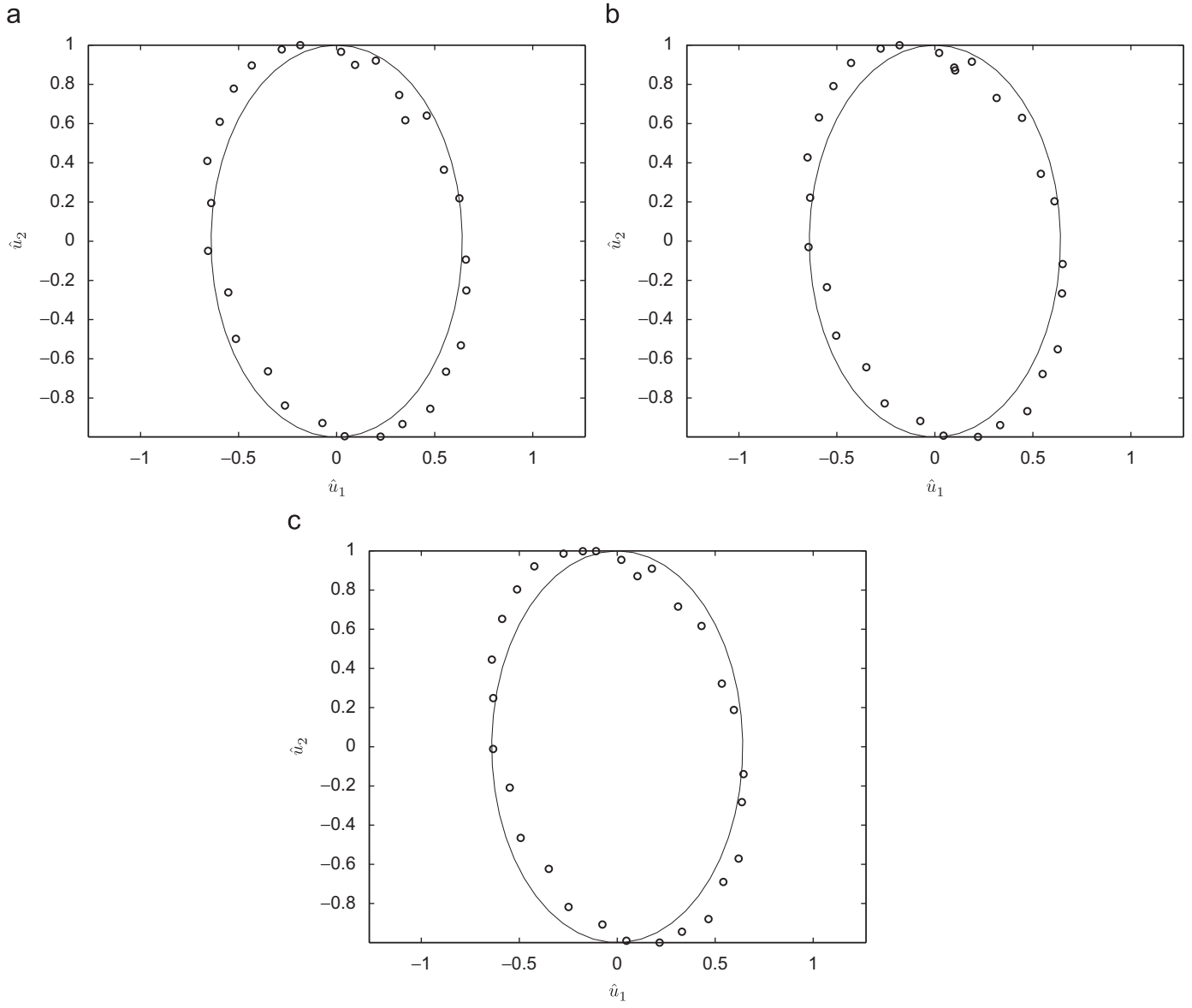

Fig. 10. Normalized trajectories evaluated at increasing distances from the source and comparison with analytical predictions (analytical—solid line, experimental—circles). (a) $x_k=2$ cm, (b) $x_k=3$ cm and (c) $x_k=4$ cm.

where $\|\tilde{u}_2(x_k,t)\|$ is the amplitude of the out-of-plane response at the considered location and time instant. The estimation of such amplitude at any generic instant of time relies of the evaluation of the analytic signal corresponding to $u_2(x_k,t)$, which is estimated through the application of the Hilbert Transform

$$\tilde{u}_2(x_k,t) = u_2(x_k,t) + j\mathcal{H}[u_2(x_k,t)], \quad (17)$$

where $\mathcal{H}[\cdot]$ denotes the Hilbert Transform.

Fig. 10 compares the analytical, shown as the solid lines, and the experimental trajectories, represented as a sequence of dots. The experimental results correspond to the response recorded at three different locations near the source. The excellent match with the analytical predictions, which confirms the validity of the experimental technique for the estimation of the displacement components, and of the signal processing procedures used for the separation of the desired wave mode, as well as for the reduction of the influence of noise.

3.5. Polarization plots for shot-peened samples

Recently, numerical studies have demonstrated that wave polarization is strongly affected by the presence of a state of prestress. In particular, Rayleigh wave polarization appears to be an order of magnitude more sensitive than the corresponding wave speed [4]. Its estimation may make the application of ultrasonic techniques for residual stress estimation an attractive approach. The measurement of multi-component wavefield data provides the experimental means for the evaluation of surface wave polarization, and therefore lends practicality to the concept. The feasibility of the approach has been demonstrated by comparing Rayleigh wave polarization in aluminum specimens which were surface-treated with three levels of shot peening intensity. The preliminary results presented in what follows show definite variations of the polarization in terms of the shot-peening intensity.

Specifically, polarization measurements are performed on specimens subjected to shot-peening treatment at 0 (untreated specimen), 8A and 16A (A-Almens). Comparison of the recorded polarization trajectories show significant differences in the relative amplitude of the surface displacement components, and in their phase, as indicated by the different orientations of the main axis of the elliptical trajectories (Fig. 11). In Fig. 11 the markers represent points estimated experimentally, while the continuous lines correspond to interpolating ellipses defined by the experimental data. The orbit for the untreated sample is identified by the red circles and the associated red dashed line corresponds to the ellipse interpolating the experimental points. Also, the black square interpolated by the solid black line correspond to the 8A sample, while the blacks dots and the dash-dot line identify the results for the 16A specimen. All of the results are found for a measurement recorded at 2 cm from the source, and for data processed according to the procedure described in Section 2.

The marked differences in the polarization plots for the three specimens suggest the need for further development of the concept, which may lead to the application of the wave polarization technique for non-destructive, non-contact characterization of surface treatment processes, and/or for the identification of residual stresses, possibly due to plasticity resulting from excessive loading.

4. Conclusions

This paper presents procedures and experiments conducted to recover both in-plane and out-of-plane displacement/velocity components of the Rayleigh wave by performing two measurements at two different incident angles. In order to separate different modes and eliminate experimental noise, the full wavefield is recorded using a single beam SLDV. The approach is validated by estimating the wave polarization trajectories (plots of in-plane versus out-of-plane displacement at a given location) and comparing the results with analytical models. For the Rayleigh waves, the major axis of the ellipse is perpendicular to the free surface whereas, the minor axis is parallel to the direction of wave propagation. Measurements on surface treated specimens show significant variations in the polarization characteristics, which suggests the possibility of using the current measurement procedure to assess the state of residual stress on the surface of the component under consideration.

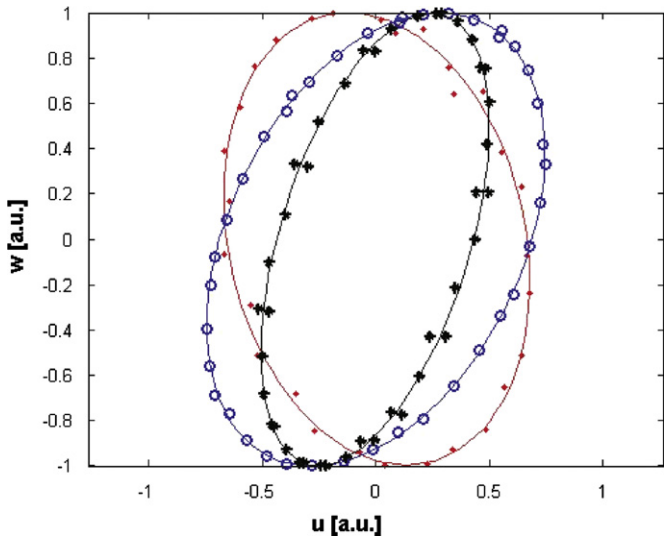

Fig. 11. Estimated trajectories for different shot peening intensities (untreated—red dashed line and red circles, 8A solid black and black squares, 16A dash-dot line and black dots). (For interpretation of the references to colour in this figure legend, the reader is referred to the web version of this article.)

Acknowledgements

The work is supported by funds from the Georgia Tech-Boeing strategic alliance on Aerospace Manufacturing for the 21st Century.

References

[1] Crecraft D. Ultrasonic wave velocities in stressed nickel steel. Nature 1962;195:1193–4.
[2] Toupin R, Bernstein B. Sound waves in deformed perfectly elastic materials. Acoustoelastic effect. Journal of the Acoustical Society of America 1961;33(2):216–25.
[3] Pao Y, Sachse W, Fukuoka H. Acoustoelasticity and ultrasonic measurements of residual stresses. Physical Acoustics 1984;17:61–143.
[4] Junge M, Qu J, Jacobs L. Relationship between Rayleigh wave polarization and state of stress. Ultrasonics 2006;44(3):233–7.
[5] Miklowitz J. Theory of elastic waves and waveguides. North Holland; 1978.
[6] Hirao M, Fukuoka H, Hori K. Acoustoelastic effect of Rayleigh surface wave in isotropic material. Journal of Applied Mechanics 1981;48:119–24.
[7] Duquennoy M, Ouaftough M, Ourak M. Ultrasonic evaluation of stress in orthotropic materials using Rayleigh waves. NDT & E International 1999;32(4):189–99.
[8] Duquennoy M, Ouaftough M, Qian M, Ourak M. Ultrasonic evaluation of stress in orthotropic materials using Rayleigh waves. NDT & E International 2001;34(5):355–62.
[9] Staszewski W, Boller C, Tomlinson G. Health monitoring of aerospace structures. Smart sensors and signal processing. Wiley and Sons Ltd; 2004.
[10] Ruzzene M. Frequency/wavenumber filtering for improved damage visualization. Smart Materials and Structure 2007;16:2116–29.
[11] Gokhale S, Hurlebaus S. Monitoring of the stress free temperature in rails using the acoustoelastic effect. In: Thompson DO, Chimenti DE, editors. Review of quantitative nondestructive evaluation, vol. 27, 2008, p. 1368–73.
[12] Schubert L, Barth M, Klesse T, Kohler B, Frankenstein B. Guided elastic waves and their impact interaction in CFRP structures characterized by 3D laser scanning vibrometry, Health monitoring of structural and biological systems. Proc. of SPIE 2008;6935:69350G.
[13] Graff K. Wave motion in elastic solids. Dover; 1991.